Colossal permittivity of (Mg + Nb) co-doped TiO_2 ceramics with low dielectric loss

Chao Yang, Mei-Yan Tse,[b] Xianhua Wei *[a] and Jianhua Hao*[b]

A high dielectric loss is one of the difficulties that hinder the application of colossal permittivity (CP) materials. Here we report the CP behaviors in ceramics of rutile (Mg + Nb) co-doped TiO_2, *i.e.*, $(Mg_{1/3}Nb_{2/3})_xTi_{1-x}O_2$. The room-temperature dielectric properties of the pure homogenous ceramics include a relatively high CP ($\varepsilon' \approx 10^4$) and an acceptable dielectric loss (0.1) at frequencies from 10^2 to 10^5 Hz in the doping concentration range of 0.5% to 7%. In particular, an excellent low dielectric loss of 0.0083 and a high dielectric permittivity of 3.87×10^4 at 1 kHz were obtained for the 1% doped sample. Moreover, the temperature stability (room temperature 180 °C) and frequency stability (10^2–10^5 Hz) of the CP properties were studied. X-ray photoelectron spectroscopy suggests that the superior CP properties could be explained by the electron-pinned defect-dipole mechanism.

The search for colossal permittivity (CP) materials is one of the hottest topics in the field of dielectrics due to their potential application in microelectronic devices and high-energy-density storage.[1,2] Some candidates have been proposed, such as perovskite ferroelectric oxides, $CaCu_3Ti_4O_{12}$, doped NiO, and $La_{2-x}Sr_xNiO_4$.[3–7] Unfortunately, these classes of materials seem to be not ideal for straightforward application. It is because they cannot meet all four requirements, including high CP, low dielectric loss , and nearly temperature- and frequency-independent dielectric properties. For example, $CaCu_3Ti_4O_{12}$ displays an extremely large loss over 20%, while ferroelectric oxides show high temperature dependent dielectric properties in the vicinity of phase transition temperature. Recently, a new CP material, (In + Nb) co-doped rutile TiO_2, satisfying the above requirements was discovered by Liu's group.[8] Different explanations have been offered for the CP mechanisms of co-doped TiO_2 including electron-pinned defect-dipole (EPDD) clusters,[8] grain-boundary effects,[9,10] hopping conductivity,[11] interfacial electrode polarization,[12] and microscopic inhomo- geneities and polaronic relaxation.[13] Although the mechanism remains debated, it has been established that the CP should arise from the defect in ceramics, not bulk materials. The dielectric polarizations of CP materials reported have been based on different host materials and involving defects formed in these hosts.[8,14,15] It also indicates the complexity and sensitivity of polarization mechanisms of defect mediated CP materials. Therefore, it is essential to widely investigate the CP properties of co-doped TiO_2 through the combination of substituted ions.

Until now, CP properties have also been confirmed in a series of rutile TiO_2 ceramics obtained by co-doping trivalent acceptors (In, Pr, Dy, Sm, Gd, Yb, Ga, Al, Er or Sc) and

pentavalent donors (Nb, Sb, or Ta).[16–23] These trivalent ions are mainly rare earth or group IIIA metals. Rare earth ions with an excessively larger ionic radius than the Ti ion would easily induce secondary phases.[20] It can be explained by the Hume- Rothery rule that a substitutional solid solution requires the mismatch of ionic radii less than 15% between doped and host ions. The rule has not been considered in doped CP TiO_2 systems, but in doped TiO_2 photocatalysts.[24] In addition, although Al, Ga, and In are from the same IIIA group, the CP of (Ga + Nb) co-doped TiO_2 originates from polaron-like behavior and a surface barrier layer capacitor effect, which is different from EPDD as is (In + Nb) co-doped TiO_2 or a compositional gradient profile as in the case of (Al + Nb) co-doped TiO_2.[8,17,18] It can be explained by different local chemistry environments like apparent valence due to different sizes of the acceptor ions. Very recently, an ultralow dielectric loss of 0.002 has been found in (In + Ta) co-doped TiO_2.[25] Such a higher performance CP property through the EPDD effect can be related to a stronger localization of electrons than that in the (In + Nb) co-doped system. It is because the Ta ion possesses one more electron shell than the Nb ion although the two ions have the same radius. These results suggest that the radius, valence, and electronic shell structure of doping ions should play important roles in CP effects. Actually, in some piezoelectrics like $(1-x)Pb(Mg_{1/3}Nb_{2/3})O_3–xPbTiO_3$ and $(1-x)Pb(Zn_{1/3}Nb_{2/3})O_3–xPbTiO_3$, the ions of Mg (Zn), Nb, and Ti occupy the octahedrally coordinated B sites.[26,27] As for rutile TiO_2, the titanium cations are also surrounded by an octahedron of six oxygen atoms, which is flexible for co-doping those ions into the lattice. Furthermore, CP properties were found in (Zn + Nb) co-doped TiO_2 with different phase structures (from the amorphous, anatase to rutile phase) in our recent works.[28] Zn belongs to group IIB, while Mg in group IIA has a closer ionic radius to that of Ti (r_{Ti} = 74.5 pm, r_{Mg} = 86 pm, r_{Zn} = 88 pm). Both of them have been reported to be helpful in decreasing the microwave dielectric loss when individually doped into TiO_2.[29] In this paper, we therefore present the structural analysis and characterization of the dielectric properties of (Mg + Nb) co-doped rutile TiO_2. The co-doped system exhibits excellent CP properties with a low dielectric loss below 0.01. Moreover, the temperature stability and frequency stability of the CP properties were studied. The physical mechanisms were also discussed.

Experimental

Co-doped samples with nominal composition $(Mg_{1/3}Nb_{2/3})_xTi_{1-x}O_2$ (x = 0.5–10%) were prepared by a conventional solid state sintering method. The raw materials used in this work were rutile TiO_2(99.99%), Nb_2O_5 (99.99%), and MgO (99.99%). Firstly, these powders were carefully weighed according to their stoichiometric amounts. Secondly, the mixing and grinding processes were carried out by ball-milling using zirconia balls for 8 h in ethanol. After all of the mixed powders were calcined at 1000 1C for 4 h in air, the dried powders incorporating polyvinyl alcohol (PVA) binder solution were pressed into pellets with a diameter of around 12 mm and a thickness of 2.0 mm by uniaxial compression. These disk samples were

sintered at 650 1C for 6 h in air for burning out the PVA binder. Finally, the samples were sintered at 1400 1C for 10 h in air and then the samples were furnace-cooled to room temperature to obtain dense ceramic samples with a relative density of about 96%. Additionally, the sintered ceramics were pasted with silver on both sides and annealed at 650 1C for 20 min in air. The phase structures of the ceramics were confirmed by X-ray diffraction (XRD) with Cu Ka (l = 0.154 nm) radiation (SmartLab, Rigaku). The vibrational properties were characterized by Raman spectroscopy (Jobin-Yvon HORIBA, HR800) with 488 nm laser excitation. Scanning electron microscopy (SEM, Tescan MAIA3) was employed to examine the surface morphologies, and elemental mapping of the sintered samples. XPS analysis was conducted on the system of a Thermo SCIENTIFIC ESCALAB 250Xi with monochromatic Al Ka radiation (1486.8 eV) for analyzing valence states of elements in the materials. An impedance analyzer (HP 4294A, Agilent) was used to evaluate the frequency dependence of dielectric properties over the range of 10^2 to 10^5 Hz. The permittivity at 1 kHz was measured as a function of temperature using a LCR meter (Agilent E4980A, Agilent) and a temperature-controlled probe stage (Linkam TS1500E, Linkam Scientific Instruments Ltd).

Results and discussion

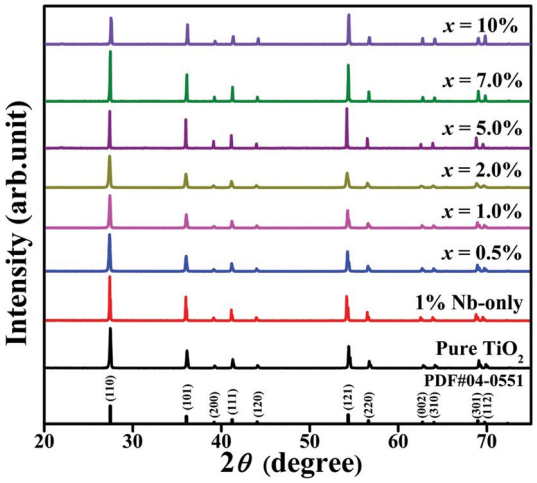

Fig. 1 XRD patterns of $(Mg_{1/3}Nb_{2/3})_xTi_{1-x}O_2$ (x = 0.5%, 1%, 2%, 5%, 7%, 10%), 1% only Nb-doped and pure TiO_2 ceramics. It was noted that the shoulders were caused by the Cu Ka_2 component.

Fig. 1 shows the XRD results of the $(Mg_{1/3}Nb_{2/3})_xTi_{1-x}O_2$ ceramics in the 2y range of 201 to 751. The ceramics were clearly observed to be made up of a pure rutile phase at different doping (Mg + Nb) contents, without any secondary phase. It was reported that the diffraction peaks of MgO can be observed even at a 2 wt% MgO content in (Ba,Sr)TiO_3–MgO composite ceramics.[30] But no information about secondary phases can be found even at the highest doping level of 10% in our work from the XRD results. It suggests that the solid solution limit of (Mg + Nb) into TiO_2 should exceed 10%. In the cases of (Zn + Nb), (Er + Nb), and (Bi + Nb) co-doped ceramics, secondary phases can be observed at a higher doping level.[16,20,28] For example,

two micro- structure regions can be found with different grain sizes and phase compositions from the SEM results of (Er + Nb) co-doped samples.[20] Besides, the distribution of the non-homogeneous phase composition increased with doped content. The presence of secondary phases could increase the dielectric loss, which can be revealed in (Bi + Nb) co-doped systems.[16] A pure phase rutile structure with a relatively high doping concentration in (Mg + Nb) could be interpreted by a closer ionic radius of Mg (86 pm) to Ti (74.5 pm) than Zn (88 pm), Er (103 pm), and Bi (117 pm). Based on the Hume-Rothery rule, a substitutional solid solution is most likely to be formed if the mismatch of ionic radii is less than 15% and the electronegativities of two elements are similar.[24] In other words, if the ionic radii of doping elements into TiO_2 are beyond the thresholds (o63 pm, or 486 pm), an interstitial solid solution or a secondary phase could be formed. Compared with In (94 pm), Zn and all rare earth ions with a larger ionic radius (486 pm), the Mg ion can more readily occupy the Ti lattice sites to promote the solid solution limit. Therefore, it is easy to understand the reason why rare earth ions would easily induce secondary phases, especially at a high doping level. Additionally, there is a small shift towards a low diffraction angle as the doping content increases, which is ascribed to the doping of Mg^{2+} and Nb^{5+} ions into the TiO_2 host lattice, resulting in an increased lattice strain.

Fig. 2 presents the Raman spectra of the sintered (Mg + Nb) co-doped TiO_2 ceramics at different doping levels. There are four Raman active fundamental modes in pure rutile TiO_2: B_{1g} (143 cm^{-1}), E_g (447 cm^{-1}), A_{1g} (612 cm^{-1}), and B_{2g} (826 cm^{-1}).[16] The B_{1g}, E_g and A_{1g} modes are visible in all compositions, which further confirm the existence of the rutile phase. Meanwhile, it should be noted that the peak B239 cm^{-1} was a multi-phonon peak for the second-order effect.[31] It is widely believed that the peak was induced by the internal stress/strain and partial reduction of the TiO_2 grains. It might be caused by doping elements with different radii from that centered in the host lattice. No extra Raman peaks arising from other phases indicate the pure rutile TiO_2 of the doped ceramics, which is in accord with the XRD phase evaluations. The A_{1g} and E_g Raman peaks correspond, respectively, to the Ti–O stretch mode and oxygen atom liberation along the *c*-axis out of phase. As the doping level *x* increases, the two bands exhibit increased red shift, asymmetric low-frequency broadening, and decrease in the peak height-to-half-width ratio. It is thought to be induced by decreasing crystallite size.[32]

In order to understand the clear surface morphology evolutions and the distributions of the elements of the (Mg + Nb) co-doped TiO_2, the SEM images and elemental mappings were obtained, as shown in Fig. 3. All the ceramics exhibit a dense microstructure with a bimodal distribution. The average grain sizes of large coarse and small fine grains were separately observed around 20 mm and 10 mm at a doping level of 0.5%. As the doping level increases by 5%, they decreased to about 8 mm and 4 mm, respectively. The change in grain sizes with doping content is the possible reason for the evolvement of the Raman results. Additionally,

the regional elemental mapping was carried out as presented in Fig. 3(c)–(f), separately characterizing the distributions of Ti, O, Mg, and Nb in the TiO_2 matrix and determining whether there was a segregation or enrichment of elements among grains and grain boundaries. In the element mapping, grain boundaries can be observed clearly in Ti and O mapping, but none in Mg and Nb mapping. It could be due to the much lower concentrations of Nb and Mg than those of Ti and O. This result indicates that all the elements including Nb and Mg are well dispersed across the grains and grain boundaries. It is different from the case of the (Er + Nb) co-doped system.

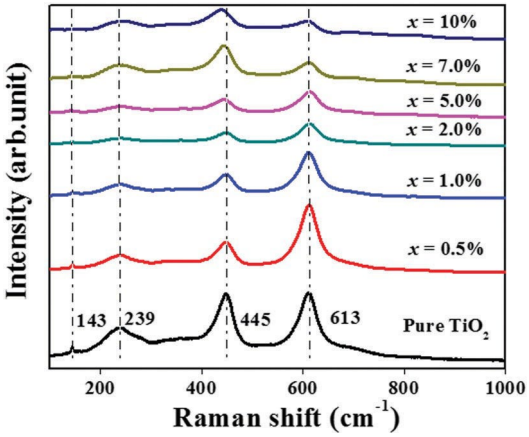

Fig. 2 Raman spectra of pure TiO_2 and TiO_2 ceramics doped with various contents of (Mg + Nb), measured at room temperature.

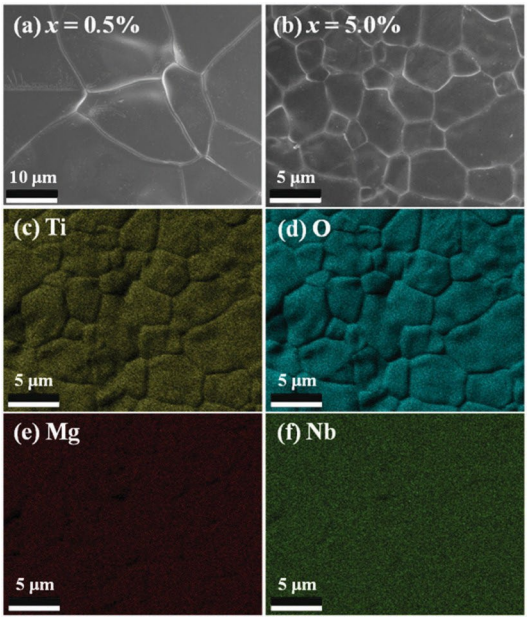

Fig. 3 Surface morphologies of the $(Mg_{1/3}Nb_{2/3})_xTi_{1-x}O_2$ ceramics with doping contents of x = 0.5% (a) and x = 5% (b), and elemental mapping of $(Mg_{1/3}Nb_{2/3})_xTi_{1-x}O_2$ ceramics at a doping level of 5 mol%: (c) Ti, (d) O, (e) Mg, and (f) Nb.

Therefore, the pure rutile TiO_2 of the doped ceramics with a dense and homogenous structure

can be confirmed due to a small mismatch of ionic radius between Mg and Ti. Fig. 4 shows the frequency dependence of the dielectric properties of (Mg + Nb) co-doped TiO_2 ceramics with different compositions. As we all know, pure TiO_2 has the largest permittivity among the unitary oxides, but is less than 260. It is noteworthy that doping only with Nb significantly increases the permittivity (4×10^4) of the host TiO_2, but the dielectric loss is mostly higher than 0.1, which is consistent with a paper reported earlier.[20]

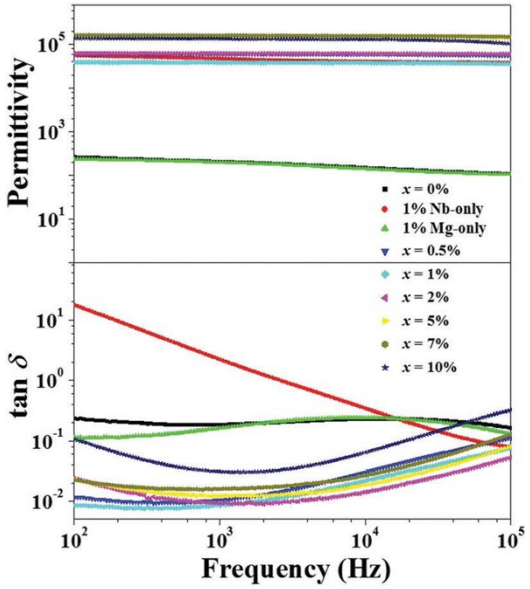

Fig. 4 Frequency-dependence of dielectric properties for (Mg + Nb) co-doped rutile TiO_2 ceramics, measured at room temperature.

On the other hand, there is no significant effect on the permittivity of doping only with Mg in TiO_2. Moreover, an enhanced dielectric behavior was found in the (Mg + Nb) co-doped ceramics. The dielectric constant is between 3×10^4 and 2×10^5, with a relatively low dielectric loss (mostly 0.1) at measuring frequencies. In particular, an excellent dielectric behavior was achieved in the ceramics with x = 1%. It would be helpful for the real application of the CP TiO_2. The dielectric loss of co-doped TiO_2 CP materials remained relatively high (40.03) before the report about the (In + Ta) co-doped system.[25] Such a low dielectric loss in this work could be explained by the same physics as EPDD. At the same time, the lowest dielectric loss (0.0074) can be found at 300 Hz for the sample. Moreover, the dielectric loss is stably lower than 0.01 below 2 kHz. The loss increases to 0.05 at about 50 kHz, and to 0.08 as the frequency is increased to 10^5 Hz. Frequency stability is achieved over a wide range for the CP properties of the (Mg + Nb) co-doped TiO_2 ceramics in the doping range of 0.5% to 7%. For the sample with a higher co-doping level of 10%, the loss will increase drastically to about 0.03–0.3 at 100 Hz to 100 kHz. The dielectric properties of the samples with high co-doping levels generally deteriorate or become uncontrollable in co-doped CP TiO_2.[9,16,20,25] It might be because the number (or probability) of those uncorrelated individual defects increases but the defects are

relatively stable.[25] In this case, the boundary layer capacitor effect would be easily observed.

To further reveal the temperature dependence of the dielectric properties, the dielectric properties of the samples were recorded at 1 kHz over the temperature range of room temperature to 475 1C, as shown in Fig. 5. For example, a stable CP was observed in the 0.5 mol% doped TiO_2 ceramics over a wide temperature range. From room temperature to 180 °C, the high permittivity and low loss can be kept stable – about 5.6×10^4 and 0.01, respectively. Besides, the significantly high-temperature dielectricrelaxation observed above 200 1C can be attributed solely to Maxwell–Wagner interfacial polarization.[8]

To explore the mechanism underlying the frequency and temperature dependence of the dielectric properties, we also obtained the XPS spectra of (Mg + Nb) co-doped TiO_2 ceramics with a 5% doping level, as introduced in Fig. 6. The peak at a binding energy of 1304.3 eV for Mg 1s implies an oxidation state of 2+ for Mg in Fig. 6(a). The XPS result in Fig. 6(b) indicates that the binding energies of Nb 3d electrons are 206.9 eV and 209.6 eV for $3d_{5/2}$ and $3d_{3/2}$, respectively, with a spin–orbit splitting of 2.7 eV. No other $3d_{5/2}$ low binding energy around

eV was found, which is consistent with that of Nb^{5+} doped TiO_2 materials.[8,20] It reveals only one Nb 3d environment in the ceramic, so that the oxidation state of this Nb is 5+.[33] Besides, the positions of the Ti 2p with $2p_{3/2}$ and $2p_{1/2}$ correspond to binding energies of 458.5 eV and 464.2 eV, respectively, which are also clearly shown in Fig. 6(c). In addition, Ti^{3+} signals were also detected with a Ti^{3+}/Ti^{4+} proportion of 3.39%, as shown in the inset of Fig. 6(c). The partial reduction of Ti^{4+} to Ti^{3+} can be explained by the introduction of Nb.

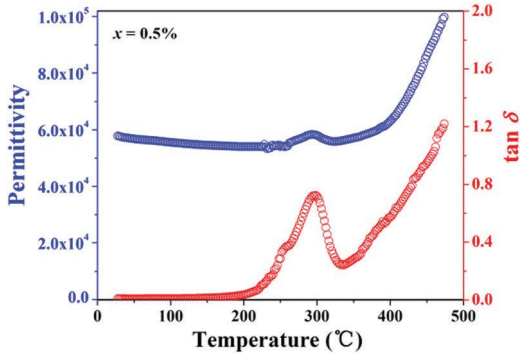

Fig. 5 Temperature-dependence (x = 0.5%, 1 kHz) of dielectric properties for (Mg + Nb) co-doped rutile TiO_2 ceramics.

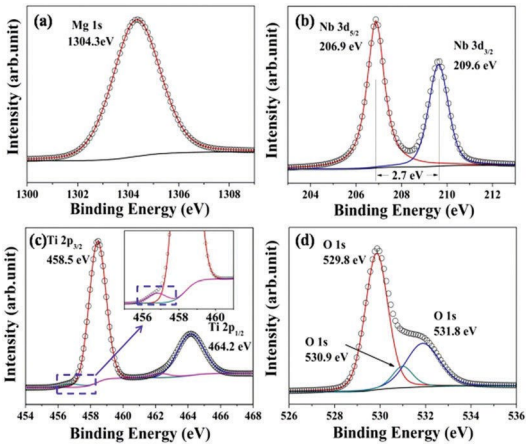

Fig. 6 Valence states of the elements in the 5% (Mg + Nb) doped TiO_2:

(a) Mg 1s, (b) Nb 3d, (c) Ti 2p, and (d) O 1s. The solid lines are fitting results. The inset of (c) is an enlarged view to clearly show the shoulders in the blue dotted boxes.

The O 1s profile in Fig. 6(d) in co-doped TiO_2 consists of three components, including 529.8 eV for bulk Ti–O, 530.9 eV associated with oxygen vacancies and surface hydroxyl (OH), and 531.8 eV for adsorbed surface H_2O. In $BaTiO_3$, the acceptor dopants of Mn or Co replacing Ti could induce a decrease in electron concentration and the formation of a defect complex[34,35] They would contribute to a lower dielectric loss or a higher resistance, which is also expected in this work. Based on the XPS results, an overall composition of $(Mg^{2+}Nb^{5+}Ti^{3+})Ti^{4+}{}_{5z}O_{2-z}$ (where $z = x/3$) can be formulated for co-doped TiO_2 as the oxygen content is assumed for charge balance. For the 5% doped sample, x can be calculated to be about 4.7% which is close to the initially weighed dopant amounts, according to the Ti^{3+}/Ti^{4+} proportion in the XPS results. The Nb^{5+}–Ti^{3+}(Ti^{4+} + e) and Mg^{2p} - $V^{\bullet\bullet}$ defect clusters are likely to have formed in the cases of Nb-only and Mg-only doped TiO_2, respectively. Considering the simultaneously observed high permittivity and low dielectric loss in co-doped TiO_2, the two defect clusters might be correlated. For the reported (Nb + In) co-doped rutile TiO_2 samples, there are two defect structures with the lowest energy configurations described as diamond and trigonal defect,[33,34] which is similar to (Zn + Nb) co-doped rutile TiO_2 ceramics.[28] As a consequence, the two types of defect clusters can be correlated/overlapped together. In this case, although Nb^{5+} doped into TiO_2 induces delocalized electrons, the introduction of Mg^{2+} produces oxygen vacancies which assist in localizing these electrons. Thus, the high CP and low dielectric loss could be acquired under the mechanism of large defect-dipole clusters with the highly localized electrons.

Interestingly, an alternative route to design low dielectric loss has been proposed through annealing the (In + Nb) co-doped TiO_2 in air.[36] Two giant dielectric responses were observed with a relatively large loss in low- and high-frequency ranges before annealing. The low-frequency dielectric response of the annealed sample disappeared by eliminating the electrode

effect and could be restored by removing the outer surface of the annealed sample. It was suggested that the internal barrier layer capacitor effect may be one of the most important factors contributing to the apparently low tan d because the conduction of free charges in a semiconducting grain can be inhibited by insulating grain boundaries. But such a low-frequency response was not found with a large permittivity and loss in this work. Therefore, the EPDD mechanism is more likely to be responsible for the observed high-performance CP in this work. Additional possible mechanisms need further investigation by changing more measuring parameters like the effect of electrode material and annealing, and the comparison of the transport properties between individual grains and within grains.[10,12,36,37]

Conclusion

In conclusion, high-performance CP performances were achieved in (Mg + Nb) co-doped TiO_2 ceramics. The ceramics showed a frequency- and temperature-stable dielectric response with a CP (410^4) and a low dielectric loss (mostly lower than 0.1). Moreover, a very low tan d of 0.0083 was found as well as a high e_r at 1× kHz in the ceramics with x = 1%. The superior performance in (Mg + Nb) co-doped TiO_2 could be explained by the EPDD mechanism.

Acknowledgement

The authors are grateful to Prof. Dunmin Lin (Sichuan Normal University) with regard to the dielectric measurements at high temperature for technical support and useful discussion. This work was supported by the Open Project of the State Key Laboratory Cultivation Base for Nonmetal Composites and Functional Materials (No. 11zxfk17). H. J. H. acknowledges financial support from the grant Research Grants Council of Hong Kong (GRF No. PolyU 153004/14P)

Notes and references

1 P. Lunkenheimer, S. Krohns, S. Riegg, S. G. Ebbinghaus, A. Reller and A. Loidl, Eur. Phys. J.: Spec. Top., 2010, 180, 61.

2 C. C. Homes and T. Vogt, *Nat. Mater.*, 2013, 12, 782.

3 M. T. Buscaglia, M. Viviani, V. Buscaglia, L. Mitoseriu,A. Testino, P. Nanni, Z. Zhao, M. Nygren, C. Harnagea, D. Piazza and C. Galassi, Phys. Rev. B: Condens. Matter Mater. Phys., 2006, 73, 064114.

4 M. A. Subramanian, D. Li, N. Duan, B. A. Reisner and A. W. Sleight, J. Solid State Chem., 2000, 151, 323.

5 C. C. Homes, T. Vogt, S. M. Shapiro, S. Wakimoto and A. P. Ramirez, Science, 2001, 293, 673.

6 J. B. Wu, C. W. Nan, Y. H. Lin and Y. Deng, Phys. Rev. Lett., 2002, 89, 217601.

7 S. Krohns, P. Lunkenheimer, C. Kant, A. V. Pronin, H. B. Brom, A. A. Nugroho, M. Diantoro and A. Loidl, Appl. Phys. Lett., 2009, 94, 122903.

8 W. B. Hu, Y. Liu, R. L. Withers, T. J. Frankcombe, L. Nor´en, A. Snashall, M. Kitchin, P. Smith, B. Gong, H. Chen, J. Schiemer, F. Brink and J. Wong-Leung, Nat. Mater., 2013, 12, 821.

9 J. L. Li, F. Li, Y. Y. Zhuang, L. Jin, L. H. Wang, X. Y. Wei, Z. Xu and S. J. Zhang, J. Appl. Phys., 2014, 116, 074105.

10 J. L. Li, F. Li, C. Li, G. Yang, Z. Xu and S. J. Zhang, Sci. Rep., 2015, 5, 8295.

11 X. G. Zhao, P. Liu, Y. C. Song, A. P. Zhang, X. M. Chen and J. P. Zhou, Phys. Chem. Chem. Phys., 2015, 17, 23132.

12 Y. L. Song, X. J. Wang, Y. Sui, Z. Y. Liu, Y. Zhang, H. S. Zhan, B. Q. Song, Z. G. Liu, Z. Lv, L. Tao and J. K. Tang, Sci. Rep., 2016, 6, 21478.

13 S. Mandal, S. Pal, A. K. Kundu, K. S. R. Menon, A. Hazarika, M. Rioult and R. Belkhou, Appl. Phys. Lett., 2016, 109, 092906.

14 Y. L. Song, X. J. Wang, X. Q. Zhang, X. D. Qi, Z. G. Liu, L. L. Zhang, Y. Zhang, Y. Wang, Y. Sui and B. Song, Appl. Phys. Lett., 2016, 109, 142903.

15 Z. J. Wang, M. H. Cao, Q. Zhang, H. Hao, Z. H. Yao, Z. H. Wang, Z. Song, Y. M. Zhang, W. Hu and H. X. Liu, J. Am. Ceram. Soc., 2015, 98, 476.

16 X. J. Cheng, Z. W. Li and J. G. Wu, J. Mater. Chem. A, 2015, 3, 5805.

17 W. Dong, W. B. Hu, A. Berlie, K. Lau, H. Chen, R. L. Withers and Y. Liu, ACS Appl. Mater. Interfaces, 2015, 7, 25321.

18 W. B. Hu, K. Lau, Y. Liu, R. L. Withers, H. Chen, L. Fu, B. Gong and W. Hutchison, Chem. Mater., 2015, 27, 4934.

19 M. Y. Tse, M. K. Tsang, Y. T. Wong, Y. L. Chan and J. H. Hao, Appl. Phys. Lett., 2016, 109, 042903.

20 M. Y. Tse, X. H. Wei and J. H. Hao, Phys. Chem. Chem. Phys., 2016, 18, 24270.

21 W. Tuichai, P. Srepusharawoot, E. Swatsitang, S. Danwittayakuld and P. Thongbai, Microelectron. Eng., 2015, 146, 32.

22 Z. W. Li, J. G. Wu and W. J. Wu, J. Mater. Chem. C, 2015, 3, 9206.

23 Z. W. Li, J. G. Wu, D. Q. Xiao, J. G. Zhu and W. J. Wu, Acta Mater., 2016, 103, 243.

24 K. Elghniji, A. Atyaoui, S. Livraghi, L. Bousselmi, E. Giamello and M. Ksibi, J. Alloys Compd., 2012, 541, 421.

25 W. Dong, W. B. Hu, T. Frankcombe, D. H. Chen, C. Zhou, Z. X. Fu, L. Cˆandido, G. Q. Hai, H. Chen, Y. X. Li, R. Withers and Y. Liu, J. Mater. Chem. A, 2017, 5, 5436.

26 T. R. Shrout, Z. P. Chang, N. Kim and S. Markgraf, Ferroelectr., Lett. Sect., 1990, 12, 63.

27 M. K. Durbin, E. W. Jacobs, J. C. Hicks and S. E. Park, Appl. Phys. Lett., 1999, 74, 2848.

28 X. H. Wei, W. J. Jie, Z. B. Yang, F. G. Zheng, H. Z. Zeng, Y. Liu and J. H. Hao, J. Mater. Chem. C, 2015, 3, 11005.

29 A. Templeton, X. R. Wang, S. J. Penn, S. J. Webb, L. F. Cohen and N. M. Alford, J. Am. Ceram. Soc., 2000, 83, 95.

30 W. B. Li, D. Zhou and L. X. Pang, J. Mater. Sci.: Mater. Electron., 2017, DOI: 10.1007/s10854-017-6600-8.

31 Y. Zhang, C. X. Harris, P. Wallenmeyer, J. Murowchick and X. Chen, J. Phys. Chem. C, 2013, 117, 24015.

32 V. Swamy, B. C. Muddle and Q. Dai, Appl. Phys. Lett., 2006, 89, 163118.

33 D. Morris, Y. Dou, J. Rebane, C. E. J. Mitchell, R. G. Egdell, D. S. L. Law, A. Vittadini and M. Casarin, Phys. Rev. B: Condens. Matter Mater. Phys., 2000, 61, 13445.

34 S. Li, H. Z. Zeng, S. Y. Zhang and X. H. Wei, Appl. Phys. Lett., 2013, 102, 153506.

35 W. J. Jie, J. Zhu, W. F. Qin, X. H. Wei, J. Xiong, Y. Zhang, A. Bhalla and Y. R. Li, J. Phys. D: Appl. Phys., 2007, 40, 2854.

36 T. Nachaithong, P. Kidkhunthod, P. Thongbai and S. Maensiri, J. Am. Ceram. Soc., 2017, 100, 1452.

37 D. A. Crandles, S. M. M. Yee, M. Savinov, D. Nuzhnyy, J. Petzelt, S. Kamba and J. Prokeˇs, J. Appl. Phys., 2016, 119, 154105.